

CONSOLIDAREA ȘI MICROSTRUCTURA COMPOZITELOR DE TIP ALUMINĂ-SiC TRATATE PRIN SISTEMUL DE SINTERIZARE CU CURENT ELECTRIC PULSAT LA TEMPERATURĂ JOASĂ

CONSOLIDATION AND MICROSTRUCTURE OF ALUMINA-SiC COMPOSITES BY THE SPARK PLASMA SYSTEM AT LOW TEMPERATURE

ENIKÖ VOLCEANOV¹, ADRIAN VOLCEANOV^{2*}

¹ Metallurgical Research Institute of Bucharest, Romania

² University Politehnica of Bucharest, Faculty of Applied Chemistry and Materials Science, Romania

The densification of pure Al_2O_3 and Al_2O_3 -SiC composites (with 5%, 10%, 20% and 30 % SiC) manufactured by the SPS process was remarkably enhanced due to additional diffusion mechanisms induced by the spark plasma even at low temperature (830 °C - 1050°C). The densification enhancement was attributed to the acceleration of the diffusion process due to additional mass-transport mechanisms induced by the spark plasma. The onset for densification of Al_2O_3 -SiC composites was delayed with increasing amounts of SiC compared with the pure Al_2O_3 compact, respectively. The delay of the densification is thought to be due to the decrease in the grain boundary and lattice diffusivity, resulting from the second phase SiC dispersion. Therefore, in the composite case, higher temperatures for fully densification should be required to supplement the decrease in the diffusivity, compared with pure Al_2O_3 . The thermal conductivity of SiC material is higher than that of Al_2O_3 , particularly at elevated temperatures and consequently, the addition of SiC might be expected to promote heat transfer from the graphite die to the compacts. Finally, the enhancement of densification for the SPS process can also be attributed by considering the additional diffusion due to Joule heating, impact force and the electric field effect in which the diffusion of ions for sintering is accelerated by an applied electric field. It is reported that the generation of spark plasma at the insulating particle-to-particle contact points enhance densification. The monoclinic moganite- SiO_2 was identified in the composite with 10% SiC particles as well as rhombohedral α - Al_2O_3 and distorted hexagonal and rhombohedral SiC polytypes. Also, a hexagonal $AlC_{0.5}O_{0.5}$ compound was revealed in the composites with 5-20% SiC and cubic Si was identified only in the composition with 30% SiC

Densificarea ceramicii aluminooase pure și a compozitelor de tip Al_2O_3 -SiC (cu 5%, 10%, 20% și 30% SiC) fabricate prin procesul SPS a fost îmbunătățită remarcabil datorită mecanismelor de difuzie suplimentare induse de sistemul de sinterizare cu curent electric pulsat (SPS), chiar la temperaturi joase (830 °C - 1050°C). Îmbunătățirea densificării a fost atribuită accelerării procesului de difuzie datorită mecanismelor suplimentare de transport în masă induse de descărcările în plasmă prin scânteie. Debutul densificării compozitelor de tip Al_2O_3 -SiC a fost întârziat de adaosurile crescânde de SiC, comparativ cu ceramica de Al_2O_3 . Se consideră că întârzierea densificării se datorează scăderii difuzivității la limita intergranulară și la nivel de rețea cristalină, ca rezultat al dispersiei SiC ca fază secundară. Prin urmare, în cazul compozitului, ar trebui să fie necesare temperaturi mai ridicate pentru o densificare completă pentru a suplimenta scăderea difuzivității, comparativ cu Al_2O_3 pură. Conductivitatea termică a carborundului (SiC) este mai mare decât cea a aluminei (Al_2O_3), în special la temperaturi ridicate și prin urmare este de așteptat ca adăugarea de SiC să promoveze transferul de căldură și de la matrița de grafit la probele compozite de consolidat. Îmbunătățirea densificării prin procesul SPS poate fi atribuită și luând în considerare difuzia suplimentară datorată încălzirii prin efect Joule, a forței de impact și a efectului câmpului electric pulsat în care, difuzia ionilor pentru sinterizare este accelerată de câmpul electric aplicat. Se raportează că generarea plasmei în scânteie în punctele de contact particule-particule izolante sporește densificarea. Moganitul- SiO_2 monoclinic a fost identificat în compozitul cu un conținut de SiC 10%, precum și polipolipuri ale SiC hexagonal și romboedric cu structuri distorsionate alături de α - Al_2O_3 . De asemenea, un compus de tip $AlC_{0.5}O_{0.5}$ cu structură hexagonală a fost evidențiat în compozitele cu 5-20% SiC, iar Si cubic a fost identificat doar în compoziția cu 30% SiC.

Keywords: Spark plasma sintering, Al_2O_3 -SiC ceramic, densification behavior, microstructure

1. Introduction

Thermal and chemical stability, relatively high resistance, low thermal and electrical conductivity, together with the availability and abundance of aluminum oxide, lead to the use in numerous engineering applications [1-5]. Despite the mentioned advantages, the reduced fracture and impact resistance of this material results in limiting its application. Composites are one of the methods

that reach this limitation. In this technique, alumina matrix is reinforced by particles or fibers as a secondary phase, which may be metal, polymer or ceramic. Silicon carbide (SiC) as a ceramic material may be one of the options leading to the improvement of the alumina matrix [6-8]. Significant attention has been attracted to Al_2O_3 -SiC composites by a pioneering work of Niihara, whose concept of nanocomposites (addition of nano-sized particles of SiC to microcrystalline alumina matrix)

* Autor corespondent/Corresponding author,
E-mail: avolceanov@gmail.com

allowed preparation of the Al_2O_3 -SiC materials with the flexural strength exceeding 1 GPa and increased fracture toughness [8]. Despite tremendous effort, the reason for such an improvement remains unclear. Niihara suggests that the strengthening arises due to the refinement of the microstructural scale from the order of the alumina matrix grain size to the order of the SiC interparticle spacing, thus reducing the critical flaw size. Strengthening can also be explained by the toughening effect caused by crack deflection due to the tensile stresses developed in alumina grains around the SiC particles as a result of thermo-elastic mismatch [8]. However, the observed toughness increase is not sufficient to account for observed strengthening. Many authors also failed to reproduce the results reported by Niihara. As a result, there exists no general agreement on the existence of the so-called "nanocomposite" effect, and alternative explanations of the observed strengthening, often related to processing or machining effects, are provided [7]. There are different methods of sintering this composite. Pressureless sintering and hot-pressing is the most common sintering method for this composite, but the new technique that is considerable today is spark plasma sintering (SPS) [5-13]. Based on the spark, which is created by a direct pulsing current, SPS leads to a rapid increase of the temperature in the powder. High heating speed, using pressure and electric current, is specific to this technique which distinguishes this technique compared to other methods. In addition to reducing the weight of the particles, the high rate of heating magnification by eliminating the surface diffusion mechanism and creating a force extracted by high temperature gradient. Applying pressure during heating can increase the driving force of the process and can facilitate the sintering process. Electric current can condense the dust by creating sparks between particles and creating the plasma environment. The SPS process involves sintering powders under the simultaneous influence of a current and pressure. The powders are placed in a mold (typically graphite) and heated is carried out by passing a current (pulsating DC current) through the mold and sample (if it is conducting) while applying pressure to the powder. The characteristics, therefore, include (a) a high heating rate; applying a pressure and (c) the effect of the current. While similar in some respects to hot pressing, the SPS process is typically characterized by a higher heating rate and current application. The effect of plasma on particle surface cleaning and improving the sintering process has been reported and particularly, the synthesis of Al_2O_3 -SiC composite by SPS has been investigated by several researchers [6,9,11], but the effect of the particles on the densification and microstructure evolution and low temperature

has not been reported so far.

2. Experimentals

2.1 Powder characteristics

The oxide component of ceramic – ceramic composites consisted of calcined alumina (ACS) with a high and fine purity, manufactured starting from aluminum hydroxide (type ALOLT-01 produced by MAL ING Aluminum Brauch-Hungary). The hydrate was moistened (mineralized) with concentrated hydrochloric acid to remove sodium ions, formed as briquettes and finally burned at 1550°C in the tunnel furnace. The slightly brittle calcined material with a content of impurities: 0.07% SiO_2 , 0.13% Fe_2O_3 and 0.01 to 0.09% Na_2O , had the chemical composition according to ICEM internal norm SF 17/1999 which allows: 0.15% SiO_2 , max. 0.20% Fe_2O_3 and max. 0.15% Na_2O .

The physical-chemical characteristics of the alumina powder are the following:

Al_2O_3 , %, 99,50
 SiO_2 , %, max. 0.15
 Fe_2O_3 , %, max. 0.20
 Alkali, %, max. 0.15
 Ignition loss, %, max. 0.20
 Humidity, %, max. 0.50
 Mineralogical composition, α - Al_2O_3 , %, min. 98,00
 Density, g/cm^3 , min. 3.70.

The oxide component of composite was alumina (ACS type) obtained by grinding in a continuous working ball mill.

A fine material with an average particle size of $2.0\ \mu\text{m}$ was obtained (evidenced by laser particle size measurements).

The non-oxide component of ceramic – ceramic composites was the carborundum (silicon carbide (SiC)) type M 600 Norton, corresponding to the β -SiC structure, 98.5% SiC, with a density of $3.00\ \text{g/cm}^3$ and an average particle size about $1.2\ \mu\text{m}$.

The alumina-SiC composites (abbreviated ACS95, ACS90, ACS80, ACS70) were obtained from alumina-carborundum mixtures according to the weight quantities presented in Table 1.

The four kinds of mixtures were milled in ethanol by a conventional wet ball milling method for 8 h. The slurries were dried at 105°C in a laboratory drier. Then the dried mixtures were ball-milled for 6 h to eliminate the agglomerates.

Powders sintering. In order to sinterise the alumina – carborundum powder an external pulsed electrical field at 1050°C - temperature with very high heating rates was applied. For SPS experiments, the mixture of powder was loaded into a graphite die with 10 mm diameter punches. After loading the powder into the die, samples were processed using a HP D 1.25 sintering machine. The samples were cured at heating rates

Table 1

Dosage of ceramic powders components/ Dozajul pulberilor ceramice componente

| Sample symbol | ACS 70 | ACS80 | ACS90 | ACS95 |
|---|--------|-------|-------|-------|
| Al ₂ O ₃ (%by weight) | 70 | 80 | 90 | 95 |
| SiC(%by weight) | 30 | 20 | 10 | 5 |

of about 200 K/min at 1050°C in a vacuum atmosphere (5×10^{-2} mbar) under a uniaxial pressure of 40 MPa was applied during sintering for all samples. After sintering for 4 min, the pressure was released and the specimens were cooled. The temperature was measured by a pyrometer (type K) on the outside wall of the die.

2.2. Characterisation methods

The relative density of the composite samples was measured by the Archimedes method in toluene medium. The density was calculated from measured mass and specimen size using a 0.1 mg error Mettler Toledo balance (AB204-S type) and a 0.001 error mm digital Mitutoyo micrometer. Mineralogical phase analyses were performed by X-ray diffraction method with parallel beam - scanning axis $2\theta / \theta$, on bulk samples. A Shimadzu XRD 6000 diffractometer with the radiation generator tube power of 1200 W, with Cu-K α characteristic radiation ($\lambda = 1,541874 \text{ \AA}$) was employed. Scanning range (2θ) of goniometry was located between 5° and 70° , with $5^\circ/\text{minute}$ angular speed and 0.02° step. The surfaces of the sintered samples were examined using a scanning electron microscope for high resolution imaging Quanta Inspect F+, equipped with an energy dispersive analysis system (EDXS).

3. Results and discussion

3.1. Densification process

In the SPS apparatus the default 12:2 (on:off) current pulsed pattern was applied. The waveform is not square and, in fact, is composed of several pulses separated by a current-free interval. Regardless of the pattern, each pulse has the same period of about 3.10^{-3} s. Thus, the pattern of 12:2 hs a sequence of 12 pulses „on” and 2 pulses with current „off”. The total time of one sequence (cycle) is about 0.04 s. The operating parameters voltage and the peak current were below 5 V and 2000 A, respectively. The typical heating power versus curing time of alumina-silicon carbide ceramic samples are given in Fig.1 and the experimental heating curve up to 1050 °C with very high heating rates is plotted in Fig.2.

Densification data of the ACS70, ACS 80, ACS 90 and ACS95 samples sintered by SPS at 1050°C with a 4 min soaking time under a pressure of 40 MPa under a vacuum atmosphere and a heating rate of 255 °C/min in the 400 - 1050 °C temperature range, as shown in Fig. 3.

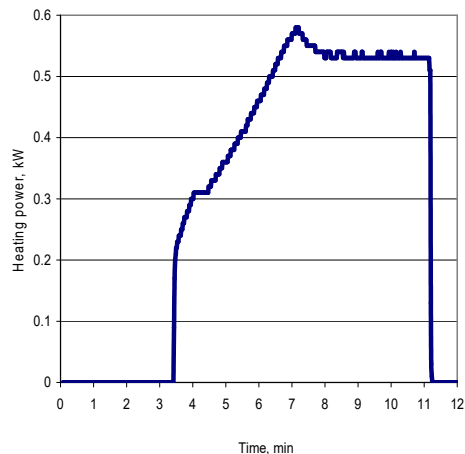


Fig.1 - Heating power by SPS versus curing time of alumina- silicon carbide composites/ Puterea de încălzire aplicată prin sistemul SPS versus timpul de tratament pentru compozitele alumino-carborundice.

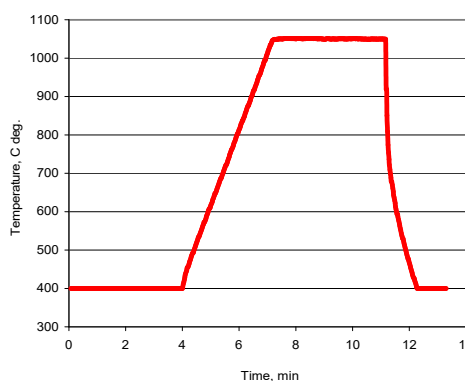


Fig.2 - Heating curve by SPS applied for the alumina-silicon carbide composites/ Curba de încălzire aplicată la tehnica SPS pentru compozitele alumino-carborundice.

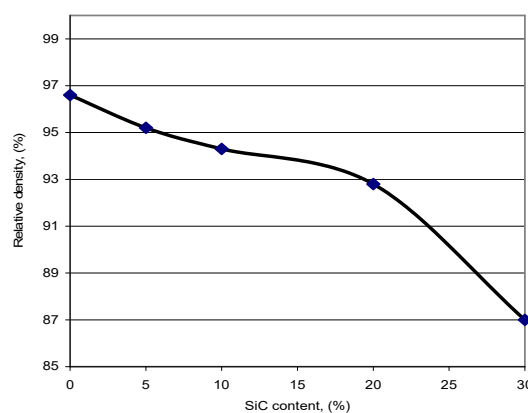


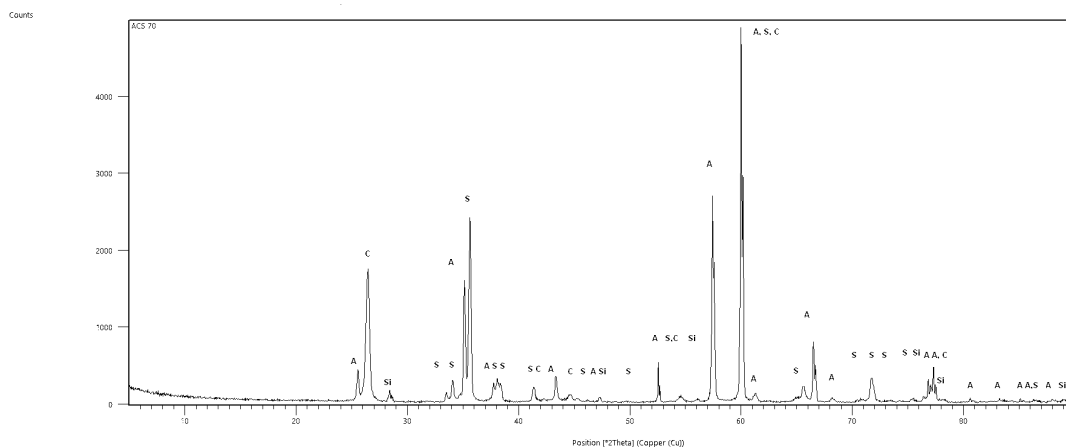
Fig.3 - Densification behaviour of alumina-SiC composites versus SiC content during the SPS treatment / Comportamentul la densificare a compozitelor alumino-SiC funcție de conținutul de SiC în timpul tratamentului SPS.

It was reported that the enthalpy energy for lattice diffusion and surface diffusion of Al_2O_3 is 578 kJ/mol [10] and 234–280 kJ/mol [14], respectively. Therefore, a rapid heating rate promotes lattice diffusion and/or grain boundary diffusion which are major densification mechanisms in the high-temperature regime rather than surface diffusion as a coarsening mechanism. Therefore, the higher heating rate which was applied to the SPS process plays an important role in enhancing the densification. Another factor affecting densification is the heat transfer from the graphite die to the sintered compacts. It can be seen that the pure Al_2O_3 composition starts to densify at about 830 °C. However, the temperatures for the onset of densification were raised by the addition of SiC. The AS95 composite (5% SiC), AS70 SiC composite (30% SiC) start to densify at about 980 and 1000 °C, respectively. So, the onset for densification of Al_2O_3 -SiC composites was delayed with increasing amounts of SiC. These results indicate that the densification process is delayed due to the addition of fine SiC particles in the Al_2O_3 matrix. This delay has been attributed to the fact the presence of SiC particles induces tensile stresses which are developed by the large thermal expansion mismatch of the components (Al_2O_3 8×10^{-6} K and SiC; 4.2×10^{-6} K) [15]. It is also thought that grain boundary and lattice diffusivity should decrease by adding SiC [16,17]. When SiC particles are located at grain boundaries in the intermediate and final stages of sintering, the grain boundary diffusion path becomes longer in proportion to the diameter of the SiC particulate, and the diffusion of atoms/vacancies along the interface between the Al_2O_3 grain and SiC particle should decrease. The observed delay of the densification, therefore, is thought to be due to the decrease in the grain boundary and lattice diffusivity, resulting from the SiC dispersion.

Therefore, in the composite case, higher temperatures for fully densification should be required to supplement the decrease in the diffusivity, compared with pure Al_2O_3 . Generally, the thermal conductivity of SiC material is higher than that of Al_2O_3 particularly at elevated temperatures. So the addition of SiC might be expected to promote heat transfer from the graphite die to the compacts. Finally, the enhancement of densification for the SPS process can also be attributed by considering the additional diffusion due to impact force, Joule heating and the electric field effect in which the diffusion of ions for sintering is accelerated by an applied electric field. It is reported that the generation of spark plasma at the insulating particle-to-particle contact points enhance densification [9]. It is not clear, however, which are the most significant parameters responsible for the enhancement of densification during the SPS process.

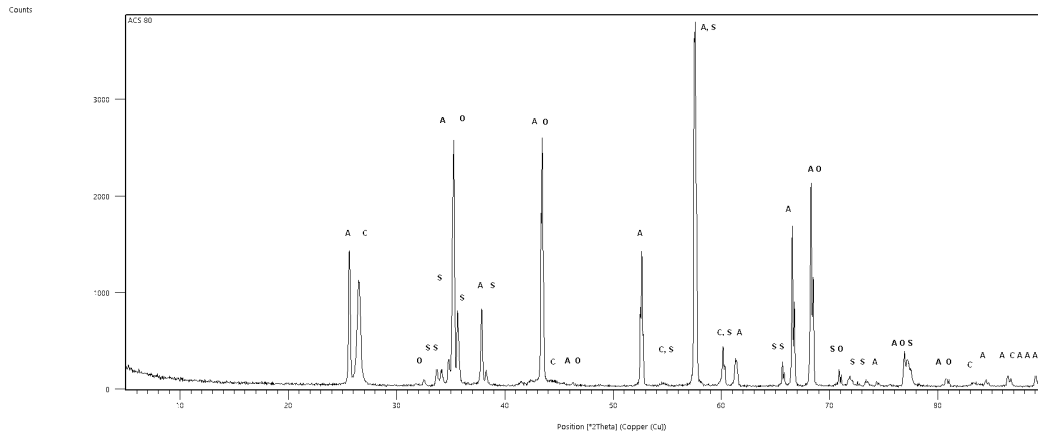
3.2. Mineralogical phases evolution

On the sample **ACS70** diffractogram as given in Fig. 4 are detectable the interferences of 3.47 (66) Å, 2.55 (100) Å, 2.37 (47) Å, 2.08 (97) Å, 1.73 (47) Å, 1.40 (35) Å, 1.37 (53) Å characteristic of rhombohedral corundum α - Al_2O_3 , respectively interference of 3.37 (100) Å, 2.13 (2) Å, 2.03 (3) Å, 1.68 (8) Å, 1.54 (2) Å, 1.23 (2) Å corresponding to graphite (carbon). Also, the presence of silicon carbide in three varieties: cubic β -SiC related to interferences 2.51 (100) Å, 2.18 (18) Å, 2.18 (18) Å, 1.54 (37) Å, 1.31 (24) Å, 1.26 (4) Å, 1.09 (4) Å, 1.00 (8) Å, 0.97 (4) Å, 0.89 (9) Å, 0, 83 (7) Å, respectively SiC moissanit -19H hexagonal with interferences of 2.51 (100) Å, 2.38 (71) Å, 2.32 (54) Å, 2.10 (17) Å, 1, 59 (20) Å, 1.53 (72) Å, 1.31 (48) Å, 2.18 (18) Å, 2.18 (18) Å, and SiC moissanite -2H hexagonal with interference of 2.35 (100) Å, 2.66 (74) Å, 2.52 (51) Å, 1.83 (23) Å, 1.53



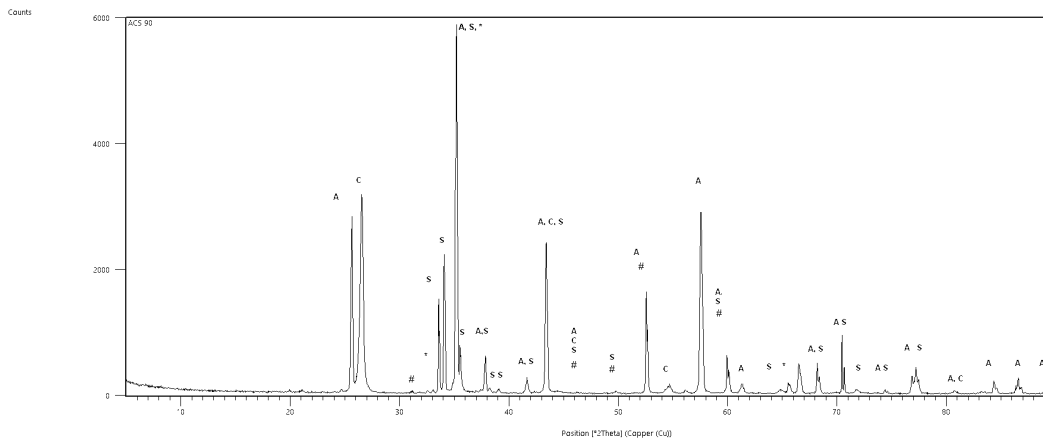
Legend/Legendă: A- Al_2O_3 , C- Carbon, S- SiC, Si- Silicium

Fig.4 - X-ray diffraction pattern of ACS 70 sample obtained by SPS / *Diffractograma probei ACS 70 sinterizate prin SPS.*



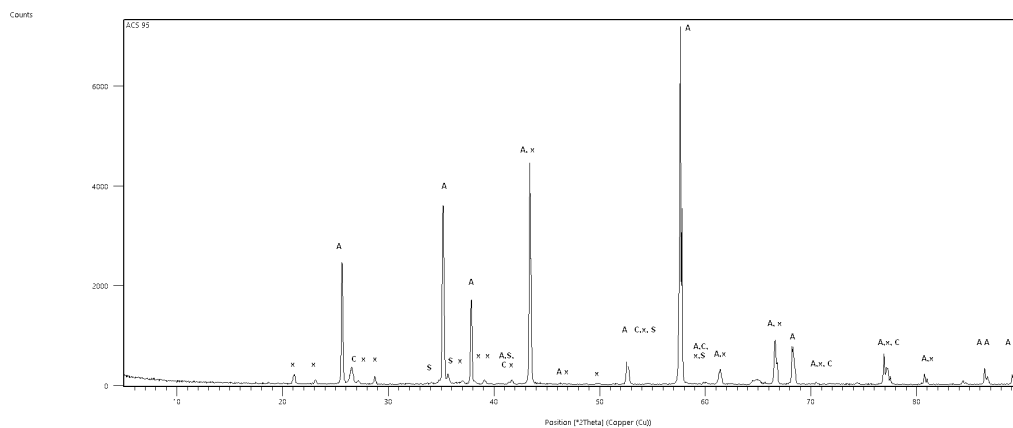
Legend/Legendă: A- Al_2O_3 , C- Carbon, S- SiC, o- $\text{AlC}_{0.5}\text{O}_{0.5}$

Fig.5 X-ray diffraction pattern of ACS 80 sample obtained by SPS /Diffractograma probei ACS80 sinterizate prin SPS.



Legend/Legendă : A- Al_2O_3 , C-Carbon, S-SiC, *- Al_2OC , #- SiO_2

Fig.6 X-ray diffraction pattern of ACS 90 sample obtained by SPS / Diffractograma probei ACS 90 sinterizate prin SPS.



Legend/Legendă: A- Al_2O_3 , C-Carbon, S-SiC, x- $\text{Al}_4\text{O}_4\text{C}$

Fig.7 - X-ray diffraction pattern of ACS 95 sample obtained by SPS /Diffractograma probei ACS 95 sinterizate prin SPS.

(24) Å, 1.42 (35) Å, 1.31 (24) Å, 1.28 (11) Å, 1.04 (9) Å were identified. Interferences of 3.13 (100) Å, 1.92 (58) Å, 1.63 (32) Å, 1.24 (10) Å, 1.10 (12) Å can be attributed to Si in cubic form resulted under reductive condition.

On the **ACS80** sample diffractogram as

seen in Fig 5 are detectable the interference of 3.47 (66) Å, 2.55 (100) Å, 2.37 (47) Å, 2.08 (97) Å, 1.73 (47) Å, 1.40 (35) Å, 1.37 (53) Å characteristic of corundum α - Al_2O_3 , rhombohedral, respectively interference of 3.37 (100) Å, 2.13 (2) Å, 2.03 (3) Å, 1.68 (8) Å, 1.54 (2) Å, 1.23 (2) Å corresponding to

the graphite. The presence of a carbide compound of aluminum oxide $AlC_{0.5}O_{0.5}$ (according to the ASTM 04-013-3673 file) with hexagonal structure was identified. Also detectable are two polytypes of SiC in hexagonal form that belong to the same space group P63mc, but differ in the volume of the elemental cell (124.06, respectively 82.82) (according to the ASTM 04-008-1656 and ASTM 04-007-1590 file), suggesting a structural distortion.

On the diffractogram of the **ACS90** sample from Fig.6, the interferences of 3.47 (66) Å, 2.55 (100) Å, 2.37 (47) Å, 2.08 (97) Å, 1.73 (47) Å, 1.40 (35) Å, 1.37 (53) Å characteristic to the corundum α - Al_2O_3 in rhombohedral form, respectively the interferences of 3.37 (100) Å, 2.13 (2) Å, 2.03 (3) Å, 1.68 (8) Å, 1.54 (2) Å, 1.23 (2) Å corresponding to graphite (carbon) can be detected. The presence of a carbide compound of Al_2OC (see ASTM file 00-036-0148) with hexagonal structure was identified. There are also two varieties of SiC, one hexagonal and one rhombohedral polytype (according to ASTM 04-002-2261 file and ASTM 04-007-1978 file). The formation of crystalline moganite-SiO₂, according to ASTM file 00-038-0360) can also be observed in monoclinic form. The presence of moganite in the treated by SPS can be explained by considering the additional diffusion due to the impact force, the Joule heating and the effect of the electric field in which the diffusion of the ion for sintering is accelerated by an applied electric field. It is reported that the generation of spark plasma at the particle-particle insulation contact points increases the densification. In this particular case, the moganite (SiO₂) is probably formed due to a reductive effect of C and the formation of SiO₂ which then reacts with O ions forming vacancies in Al_2O_3 structure. Also in this composite, the formation of an unreacted Al_2OC and C carbide compound is detected, which supports the formation of moganite, also. Moreover, it was found that the onset of densification of Al_2O_3 -SiC composites was delayed with increasing amounts of added SiC.

On the diffractogram of the **ACS95** sample from Fig. 7 the interferences of 3.47 (66) Å, 2.55 (100) Å, 2.37 (47) Å, 2.08 (97) Å, 1.73 (47) Å, 1.40 (35) Å, 1.37 (53) Å characteristic of rhombohedral corundum α - Al_2O_3 , respectively the interferences of 3.37 (100) Å, 2.13 (2) Å, 2.03 (3) Å, 1.68 (8) Å, 1.54 (2) Å, 1.23 (2) Å corresponding to graphite (carbon). The presence of a carbide compound of aluminum oxide Al_4O_4C (see ASTM file 00-049-1428) with orthorhombic structure was identified. Also, a single polytype of SiC one with hexagonal shape (according to the ASTM 04-002-2261 and ASTM 04-007-1978) can be detected.

3.3. Microstructure

The surfaces of the samples were examined using a scanning electron microscope for high resolution imaging. The results obtained are presented for each sample in the images below. The characteristic aspect of the ACS 70 ceramic samples surface, sintered by the SPS process is shown in Fig.8 – 11 with details for each component. The images show a granular structure with dimensions between 10 – 80 μm and pores. In Fig. 9, the distorted hexagonal SiC structures with dimensions of 30-70 μm were noted in major rhombohedral Al_2O_3 matrix. On the surface of the SiC granules some glassy-looking striations can be observed, probably due to the formation of SiO₂ as a consequence of SiC decomposition. A process of densification is highlighted by the formation of intergranular “bridges” in the alumina rich – see Fig.10 – 11, as a result of diffusive processes that take place in the volume of the sample. In the rich alumina area, the granules have dimensions between 10 – 80 μm . The pores are located at the intergranular border SiC- Al_2O_3 , Al_2O_3 - Al_2O_3 having dimensions of 0.1-0.9 μm and on the surface of the granules having 2-3 μm . The SPS treatment applied led to magnification of the alumina granules by 2-20 times.

The characteristic aspect of the breaking surface of the **ACS 80** ceramic samples sintered by the SPS process is shown in Fig. 12 - 15 with details for each component. The images show a structure with granules having dimensions between 14 – 67 μm and pores. In the alumina rich area – Fig. 12-13 – the grains have dimensions between 14 – 23 μm . The pores are located at the intergranular boundary SiC- Al_2O_3 , respectively Al_2O_3 - Al_2O_3 having dimensions of 5-10 μm and on the surface of the granules having 3-5 μm . A densification process is highlighted by the formation of intergranular “bridges” in the alumina rich area – see Fig. 14 as a result of diffusive processes that occur in the sample volume. The SPS treatment applied leads to growth of alumina grains of 3-17 times. In Fig.15 is shown a phenomenon of tabularization of alumina granules under rapid heating rate and the applied impact force.

The characteristic aspect of surface of the **ACS 90** ceramic samples sintered by the SPS process is shown in the images Fig.16 – 19 with details for each component. The images show a structure with granules having dimensions between 12 – 88 μm and pores. In the alumina matrix – Fig. 16-17. The pores are located at the intergranular boundary (Fig. 17) SiC- Al_2O_3 and Al_2O_3 - Al_2O_3 have dimensions of 2-16 μm and on the surface of the granules having 5-15 μm .

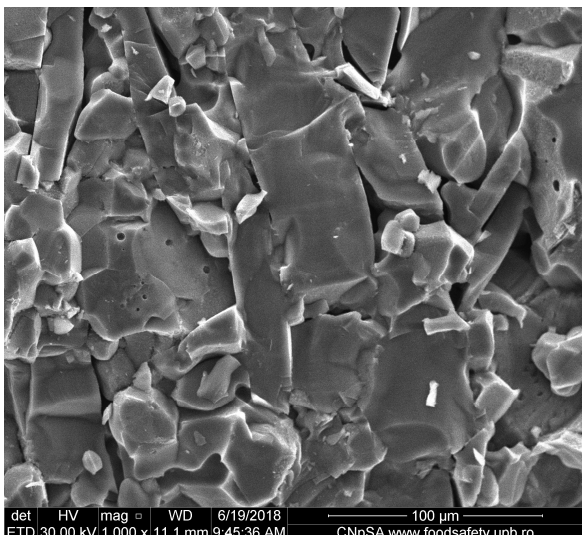


Fig.8 - Detail of ACS sample surface 70, Magnification x 1000
 Detaliu al suprafeței probei ACS 70, Mărire x 1000.

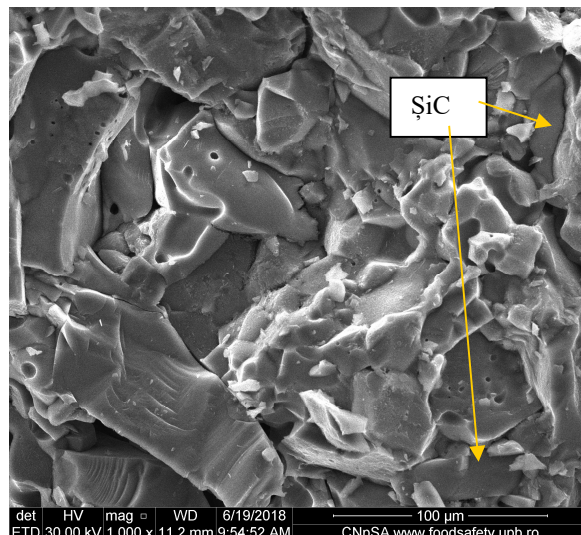


Fig.9 - Detail of ACS sample surface 70, Magnification x 1000
 Detaliu al suprafeței probei ACS 70, Mărire x 1000.

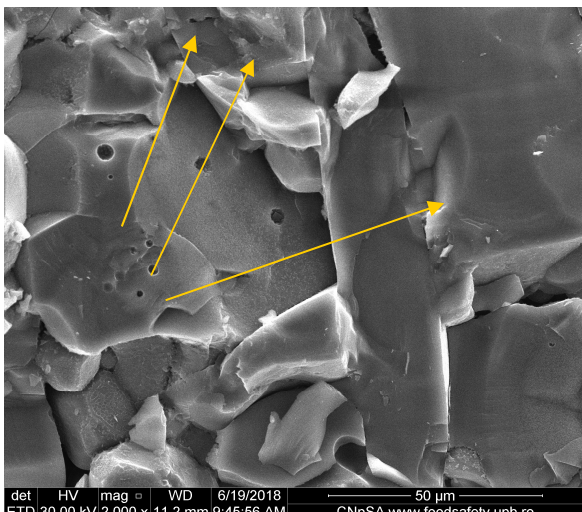


Fig.10 - Detail of ACS sample surface 70 in the alumina rich area, showing the formation of intergranular necks during sintering, Magnification x 2000 / Detaliu al suprafeței probei ACS 70 în zona aluminoasă, cu formarea unor punți intergranulare, Mărire x 2000.

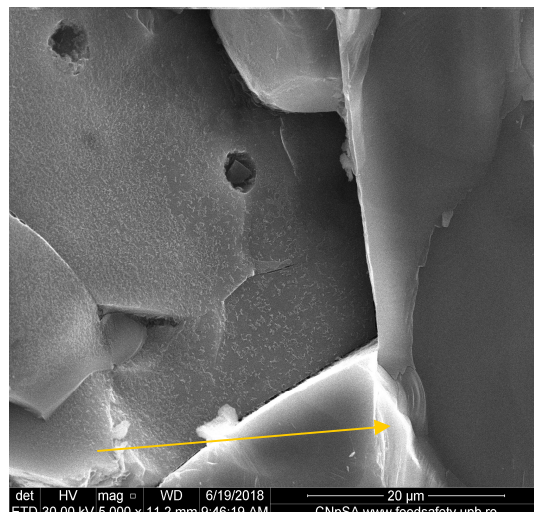


Fig.11 - Detail of the surface of the ACS 70 sample, in the alumina rich area, Magnification x 5000 / Detaliu al suprafeței probei ACS 70 în zona aluminoasă, Mărire x 5000 .

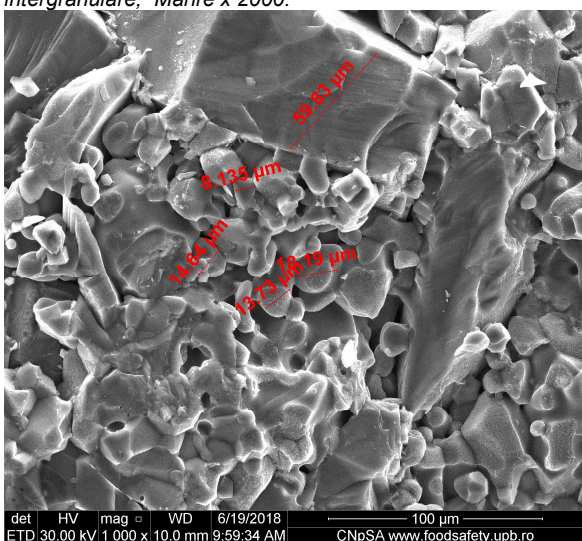


Fig.12 - Detail of ACS80 sample surface, Magnification x 1000 / Detaliu al suprafeței probei ACS80, Mărire x 1000

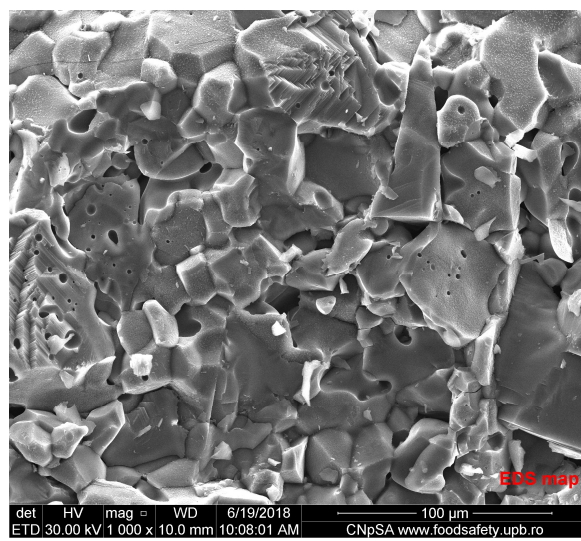


Fig.13 - Detail of the ACS80 sample surface, Magnification x 1000 / Detaliu al suprafeței probei ACS80, Mărire x 1000.

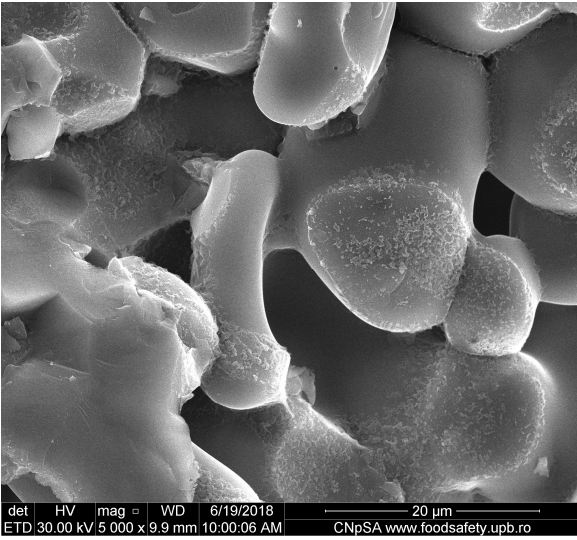


Fig.14 - ACS80 sample surface detail, Magnification x 5000
Detaliu al suprafeței probei ACS80, Mărire x 5000.

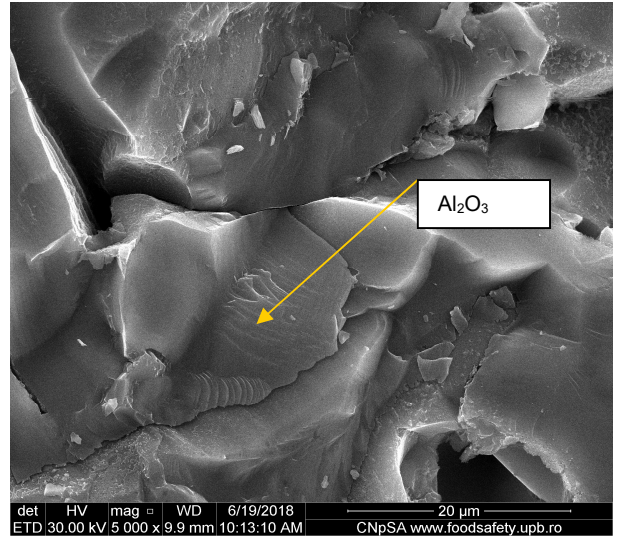


Fig.15 - Detail of ACS80 sample surface, Magnification x 5000/
Detaliu al suprafeței probei ACS80, Mărire x 5000.

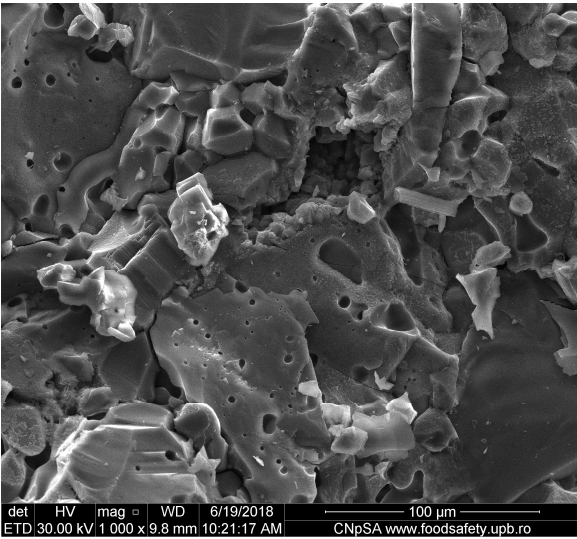


Fig.16 - ACS90 sample surface detail, Magnification x 1000
Detaliu al suprafeței probei ACS90, Mărire x 1000.

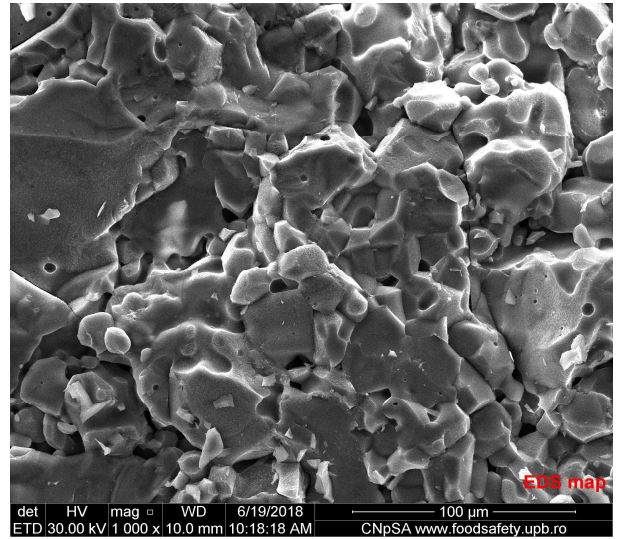


Fig.17 - ACS90 sample surface detail, Magnification x 1000
Detaliu al suprafeței probei ACS90, Mărire x 1000.

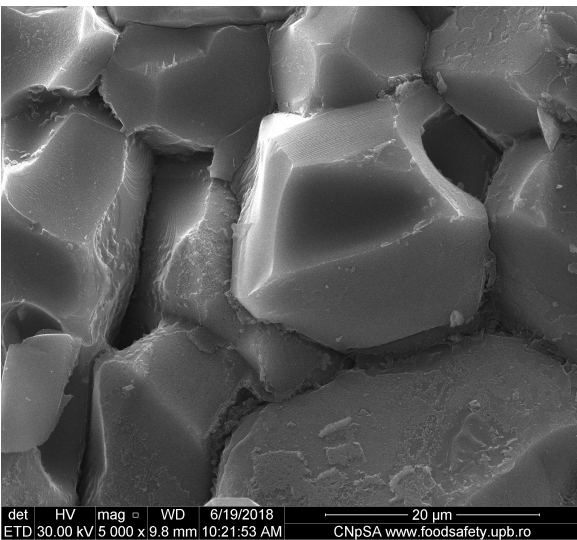


Fig.18 - ACS90 sample surface detail, Magnification x 5000/
Detaliu al suprafeței probei ACS90, Mărire x 5000.

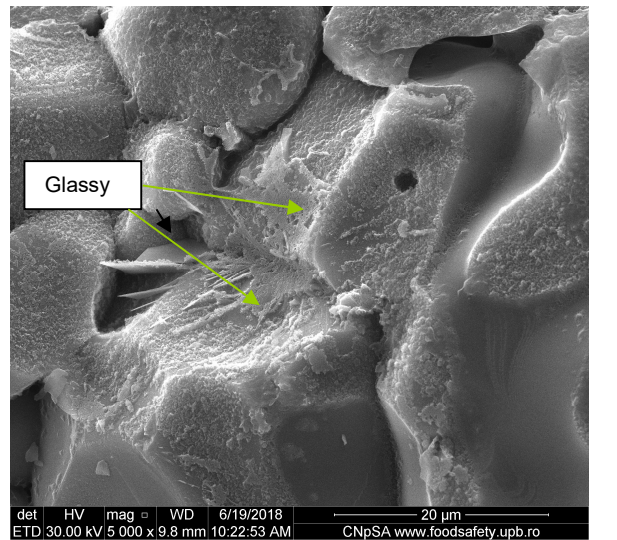


Fig.19 - Detail of the ACS90 sample surface, Magnification x 5000/
Detaliu al suprafeței probei ACS90, Mărire x 5000.

The granules of SiC respectively the presence of a small amount of glassy phase can be observed. A densification process is highlighted by the formation of intergranular "bridges" in the alumina rich area - see Fig.18 as a result of diffusive processes that take place in the volume of the sample. The SPS treatment applied led to alumina granules growth and a rounded aspect of the granules. In Fig.19, a glassy precipitate was observed on the surface of the alumina granules, probably due to the decomposition of SiC in SiO₂ (moganite) and CO and/or precipitation of AlOC. The thermal conductivity of SiC material is higher than that of Al₂O₃ particularly at elevated temperatures, the addition of SiC might be expected to promote heat transfer from the graphite die to the compacts, enhancing the additional diffusion mechanism, probably promoting the formation of moganite and Al₂OC.

The characteristic aspect of the breaking surface of the **ACS 95** ceramic samples sintered by the SPS process is shown in Fig. 20 – 23 with details for each component. The images show a granular structure with dimensions ranging from 14 to 102 μm and pores. In the alumina matrix - Fig. 20 - granules have dimensions ranging from 14 to 78 μm. The pores are located at the intergranular boundary SiC- Al₂O₃ and Al₂O₃- Al₂O₃ have dimensions of 2-16 μm as well as on the surface of the granules in 5-15 μm range. In Fig.21 the SiC granules and a rounded aspect of the granules can be observed. The densification process is highlighted by the formation of intergranular "bridges" in the alumina rich area - see Fig.22- 23 as a result of diffusive processes that take place in the volume of the sample. Magnification of the alumina granules and a rounding aspect of the granules have been recorded after SPS treatment.

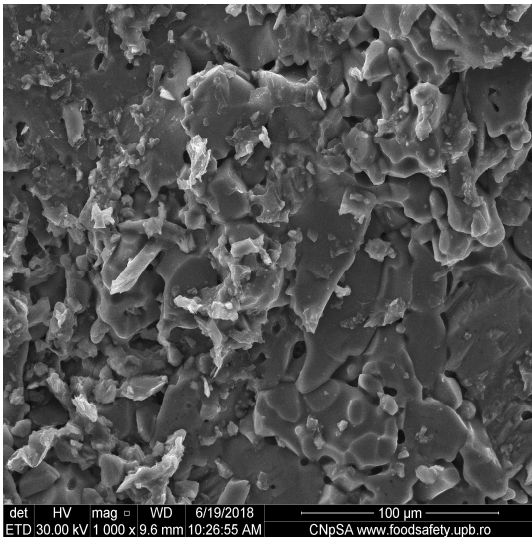


Fig.20 - Detail of the ACS95 sample surface Magnification x 1000 /Detaliu al suprafeței probei ACS95, Mărire x 1000.

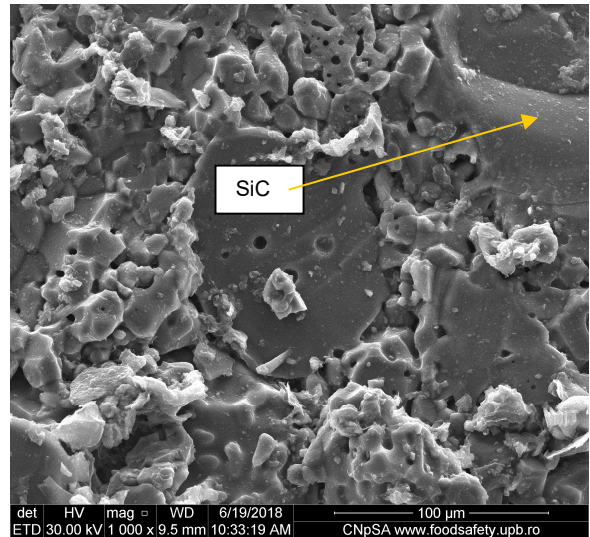


Fig.21 - Detail of the ACS95 sample surface Magnification x 1000/ Detaliu al suprafeței probei ACS95, Mărire x 1000.

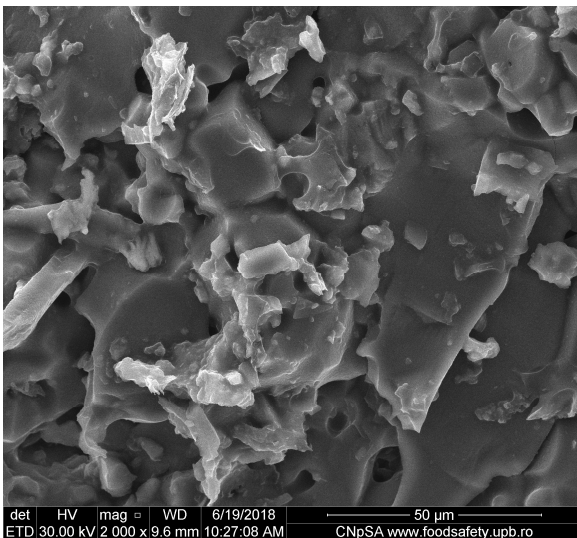


Fig. 22 - Detail of ACS95 sample surface, Magnification x 2000/ Detaliu al suprafeței probei ACS95, Mărire x 2000.

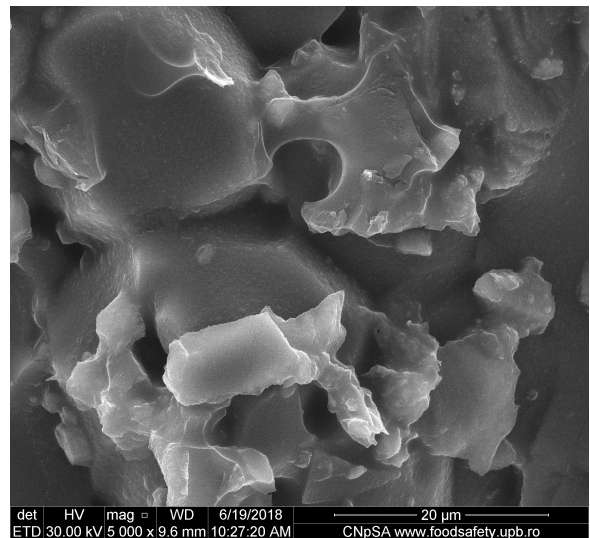


Fig.23 - Detail of ACS95 sample surface, Magnification x 5000/ Detaliu al suprafeței probei ACS95, Mărire x 5000.

The grain size of the matrix grains has been significantly reduced by the SiC dispersion because grain boundary mobility is decreased by the SiC fine particles that pin grain boundary movement. Grain boundary mobility also influences grain growth as well as densification [12-17]. There are four factors that contribute to the fast densification process in a SPS process [9] (a) the use of rapid heating and cooling rates; (b) the application of a higher mechanical pressure than that used in a conventional hot-pressing process; (c) rapid heat transfer; (d) the use of a pulsed direct current, where samples are also exposed to an electric field. The presence of SiC particles induces tensile stresses which are developed by the large thermal expansion mismatch of the components. Moreover, SiC particles, located at the grain boundaries, resist crack propagation. These two factors, which promote transgranular fracture in composite materials, increase the fracture toughness because transgranular fracture requires higher energy to propagate a crack compared with intergranular fracture. Particle bridging should be also considered an important toughening mechanism [18,19].

4. Conclusion

The sintering behavior and microstructural evolution was investigated for Al₂O₃-SiC composites sintered by a SPS process. The densification of pure Al₂O₃ and Al₂O₃-SiC ceramics manufactured by the SPS process was remarkably enhanced due to additional diffusion mechanisms induced by the spark plasma even at low temperature (830 °C - 1050°C). The observed delay of the densification, therefore, is thought to be due to the decrease in the grain boundary and lattice diffusivity, resulting from the SiC dispersion. Therefore, in the composite case, higher temperatures for fully densification should be required to supplement the decrease in the diffusivity, compared with pure Al₂O₃. It was also considered that the addition of SiC particles (5%, 10%, 20% and 30%) with a lower thermal expansion coefficient than the Al₂O₃ matrix, induced transgranular fracture, resulting in crack tip shielding, such as particle bridging and stress-induced microcracking, which acted as toughening mechanisms. One can be expected improvements in the fracture toughness and strength of Al₂O₃-SiC ceramics prepared by a SPS as this process is closely related to the densification behavior and microstructural changes, as well as the effect of the fine SiC dispersion. A rapid heating rate promotes lattice diffusion and/or grain boundary diffusion which are major densification mechanisms in the high-temperature regime rather than surface diffusion

higher heating rate which was applied to the SPS process plays an important role in enhancing the densification. Another factor affecting densification is the heat transfer from the graphite die to the sintered compacts. Usually, the thermal conductivity of SiC material is higher than that of Al₂O₃ particularly at elevated temperatures. Consequently, the addition of SiC might be expected to promote heat transfer from the graphite die to the compacts. Finally, the enhancement of densification for the SPS process can also be attributed by considering the additional diffusion due to impact force, Joule heating and the electric field effect in which the diffusion of ions for sintering is accelerated by an applied electric field leading to the insulating to particle-to-particle contact points enhanced densification. The monoclinic moganite-SiO₂ was identified in the ceramics with 10% SiC particles as well as rhombohedral α-Al₂O₃ and distortional hexagonal and rhombohedral SiC polytypes. Also, a hexagonal AlC_{0.5}O_{0.5} compound was identified in the compositions with 5-20% SiC. The cubic Si was revealed in the composition with 30% SiC.

ACKNOWLEDGMENTS:

The authors kindly acknowledge the useful help and discussion of Assist.Prof. Vasile Adrian Surdu and Research Assist. Roxana Truşcă.

REFERENCES

- [1] D. M. Constantinescu, M. Sandu, E. Volceanov, M.C.Miron, D.A. Apostol, Strength Response and Failure Analysis of Ceramic Alumina Tiles, Key Engineering Materials; Advances in Fracture and Damage Mechanics VIII, 2010, **417-418**: 673-676.
- [2] R. State, A.Volceanov, E.Volceanov, S. Stoleriu, Alumina composites obtained by unconventional heat treatment, Romanian Journal of Materials; 2011, **41**(4) 362-370
- [3] E.Volceanov, A.Volceanov, S.Stoleriu, Assessment on mechanical properties controlling of alumina ceramics for harsh service conditions, Journal of the European Ceramic Society, 2007, **27** (2-3), 759-762
- [4] Z.Shen, M. Johnson, Z. Zhao, & M.Nygren, Spark plasma sintering of alumina, Journal of the American Ceramic Society, 2002, **85** (8), 1921-1927.
- [5] E.Volceanov, G.V.Aldica, A. Volceanov, D.M. Constantinescu, S. Motoc, From conventional to fast sintering of zirconia toughened alumina nanocomposites, Mechanical Properties and Performance of Engineering Ceramics and Composites IV, Ceramic Engineering and Science Proceedings, The33rd International Conference on Advanced Ceramics and Composites; Jan. 18-23, 2009, Daytona Beach, Florida, USA, 2010, **30**(2), 91-102
- [6] M.D. Unlu, G. Goller, O. Yucel, F.C. Sahin, The Spark Plasma Sintering of Silicon Carbide Ceramics Using Alumina, Acta Physica Polonica A, 2014, **125**(2), 257-259
- [7] D.Galusek, D. Galusková, Alumina Matrix Composites with Non-Oxide Nanoparticle Addition and Enhanced Functionalities-Review, Nanomaterials, 2015, **5**, 115-143
- [8] K. Niihara, New design concept of structural ceramics—Ceramic nanocomposites, J. Ceram.Soc. Jpn. 1991, **99**, 974-982.
- [9] J.H Chae, K.H. Kim, Y.H. Choa, J.I. Matsushita, J.W. Yoon, K.B. Shim, Microstructural evolution of Al₂O₃-SiC nanocomposites during spark plasma sintering, J. Alloy Compd., 2006, **413**, 259-264

as a coarsening mechanism. Therefore, the

- [10] T.Ohji, A.Nakahira, T. Hirano, K. Niihara, Tensile creep behavior of alumina/silicon carbide nano-composite, J. Am. Ceram. Soc., 1994, **77**, 3259-3262
- [11] O.T. Johnson, P. Rokebrand, I. Sigalas, Microstructure and Properties of Al₂O₃-SiC Nanomaterials, Proceedings of the World Congress on Engineering, 2014, **2**, WCE 2014, July 2 - 4, 2014, London, U.K,
- [12] Z.A. Munir, D. Quach, M. Ohyanagi, Electric Current Activation of Sintering: A review of the pulsed electric current sintering process, J. Am. Ceram. Soc., 2011, **94**, 1-19.
- [13] M. Tokita, Spark plasma sintering (SPS) method, systems and applications, Handbook of Advanced Ceramics: Materials, Application, Processing and Properties, 2nd ed.; Somya, S., Ed.; Academic Press: Waltham, MA, USA, 2013; 1149-1178.
- [14] R.M. Cannon, R.L. Coble, Deformation of Ceramic Materials, Plenum Press, New York, 1975, p. 61
- [15] M. Omori, Sintering, consolidation, reaction and crystal growth by the spark plasma system (SPS), Materials Science and Engineering A287, 2000, 183 - 188
- [16] I. Levin, W.D. Kaplan, D.G. Brandon, A.A. Laybourn, Effect of SiC submicrometer particle size and content on fracture toughness of alumina-SiC nanocomposites, J. Am. Ceram. Soc., 1995, **78**, 254 - 256.
- [17] A. Nakahira, K. Niihara, Fracture Mechanics of Ceramics, Plenum Press, New York, 1992, p.165
- [18] K. Niihara, A. Nakahira, T. Uchiyama, T. Hirai, Fracture Mechanics of Ceramics, Plenum Press, New York, 1986, p.103
- [19] A.J. Winn, R.I. Todd, Microstructural requirements for alumina-SiC nanocomposites, British Ceram. Trans., 1999, **5**, 219-224.

MANIFESTĂRI ȘTIINȚIFICE / SCIENTIFIC EVENTS

2nd Global Congress on Advanced Composite Materials, Porto, Portugal 4 – 5 May 2020

Topics

- Composite Materials - Applications
- Materials and Innovative Processing Ideas
- Biocomposites and Biopolymers
- Crystalline Materials
- Composites Manufacturing Process Outlook
- Advanced Composite Materials and Technologies
- Marine Applications of Advanced Fibre-reinforced Composites
- Thermoplastic Polymer
- Composites fuel growth of fuel cell technology
- Composite Materials & Technology for Defence
- Electrical, Optical and Magnetic Materials
- Hydrogen Energy and Fuel Cell technology
- Advanced Graphene & 2D Materials
- Applications of Polymers in Medicine, Health and Biotechnology
- Bio-fibers and Composite Materials
- Crystallography of Novel Materials
- Novel materials for Energy applications
- Functional Materials
- Multifunctional composites
- Polymer matrix composites
- Metal Matrix Composites
- Ceramic Matrix Composites
- Future of Thermoplastic Composites
- New Composite Prevents Metal Corrosion in Extreme Conditions
- Computational Materials Science
- Magnetic Nanostructures
- Energy Harvesting Materials
- Polymers Electrochemistry
- Applications in Medicine
- Fibrous & Particulate Composites
- Recycling technologies for thermoset composite materials
- Self-healing Composites
- Molecular Dynamics Modeling of Materials
- Material Behavior of Lightweight Alloys
- Porous Materials
- Photonic Materials
- Spintronic Materials
- Meta materials
- Concrete and cementitious composites
- Nanobiotechnology
- Carbon fiber reinforced polymer and Its Applications
- Composite Materials in Aerospace Applications
- Soft Materials
- Mechanical and physical properties of composite materials
- Hybrid Composites
- Thermosetting Polymer organic and inorganic composites
- Advanced synthetic polymers
